Grid-Array Rectenna With Wide Angle Coverage for Effectively Harvesting RF Energy of Low Power Density

Yi-Yao Hu, *Student Member, IEEE*, Sheng Sun, *Senior Member, IEEE*, Hao Xu, and Hucheng Sun, *Member, IEEE*

***Abstract*— It is difficult to effectively rectify or convert low power in the circuit stage of harvesters. The high-gain antenna can offer a higher level of power and is beneficial to RF power harvesting in a low power density environment. To extend the narrow beam of the conventional high-gain rectenna, the multiport and multibeam antenna is promising. To pursue a simple configuration and avoid extra beamforming networks, a traveling-wave grid-array antenna (GAA) with two isolated ports and two symmetrically tilted beams is proposed. A prototype is designed and fabricated after a detailed analysis of the GAA with tilted beams and the coplanar stripline-based rectifier. The measured results show that the proposed rectenna is sensitive and effective in a wide-angle range. The harvesting angle range is extended by combining two tilted beams and can be greater than 70°, where the level of dc power exceeds 100 μW when the power density is as low as 1 μW/cm^2. A maximum dc output of 3.6–203.8 μW and a maximum RF-to-dc conversion efficiency of 16.3%–45.3% are available at 2.45 GHz, under the condition that the power density ranges from 0.052 to 1 μW/cm^2.**

***Index Terms*— Energy harvesting, grid-array antenna (GAA), high gain, multibeam, rectifying antenna, wireless power transfer (WPT).**

I. Introduction

With the emergence of the smart environment concept, the management of homes, factories, and cities could be more intelligent. As the basic element of intelligence, the sensors will be extensively installed to form a network, for detecting changes of environment, including temperature, moisture, vibration, and pressure. Benefited from increasingly lower levels of power consumption, one battery could power a sensor node for several years; however, the maintenance of such amount of sensor nodes will be labor intensive and time-consuming when batteries run out or unexpectedly fail to supply power. It could be solved by the technique of RF energy harvesting, which can be complementary to the battery in a reliable system, and even alternative in some low-power scenarios [1]–[5]. Different from other ambient energy sources such as light and wind, the indoor and outdoor RF energies are emitted from widespread RF transmitters such as Wi-Fi routers and base stations in an urban area and can be continuously detected. In addition, RF energy harvesting employs the rectenna, which consists of an antenna and a rectifying circuit, and then is more compatible with the wireless communication system. The RF power harvester research has shown that harvesting and communication can share a set of antennas [1]–[3], [5], [6]. However, RF energy harvesting is not easy to implement effectively. In fact, the power density of ambient RF energy is very low [7]–[10], and probably leads to a low level of collected RF power. Limited by the rectifying devices including frequently used Schottky diodes, transistors, and CMOS schemes, low input RF power will cause a poor RF-to-dc conversion efficiency, which becomes the major obstacle to the RF energy harvesting [11], [12].

In recent years, research studies pursuing high efficiencies have been conducted from different perspectives.

The spindiode and the backward tunnel diode were explored to break through the limitation of rectifying devices in the low power regime [11], [12]. The optimal impedances of the diode and dc load were analyzed under a range of low power density [13]. Signal waveforms were studied and optimized to enhance the rectifying efficiency in [14] and [15]. Harmonics were terminated and recycled in class-C, class-F, and inverse class-F rectifiers [16]–[18]. The dc–dc converters such as boost and buck-boost converters were designed for emulating optimal resistive loads to maximize the efficiency [19]–[22], and a startup circuit with a charge pump was implemented for dc–dc stage in a low-voltage and low-power regime in [20]. Resistance compression networks were adopted in rectifier designs to reduce the sensitivity to the variations of the load and input power [23]–[26]. Rectifier topologies of Greinachar and stacked voltage doublers were introduced into broadband [8], [24] and multiband [10], [27], [28] applications. By combining different rectifiers [29], integrating rectifying devices with switches [30]–[32], or using hybrid couplers [33], a high efficiency can be maintained in a wider range of power. Eliminating the matching circuit between the rectifying circuit and the antenna was recommended to avoid additional losses [34], [35].

Manuscript received May 15, 2018; revised August 8, 2018; accepted October 16, 2018. Date of publication December 3, 2018; date of current version January 4, 2019. This work was supported in part by the National Natural Science Foundation of China under Grant 61622106 and Grant 61721001 and in part by Sichuan Science and Technology Program under Grant 2018RZ0142. *(Corresponding author: Sheng Sun.)*

Y.-Y. Hu, S. Sun, and H. Xu are with the School of Electronic Science and Engineering, University of Electronic Science and Technology of China, Chengdu 611731, China (e-mail: sunsheng@ieee.org).

H. Sun is with the Research Center of Applied Electromagnetics, Nanjing University of Information Science and Technology, Nanjing 210044, China.

Color versions of one or more of the figures in this paper are available online at http://ieeexplore.ieee.org.

Digital Object Identifier 10.1109/TMTT.2018.2881127

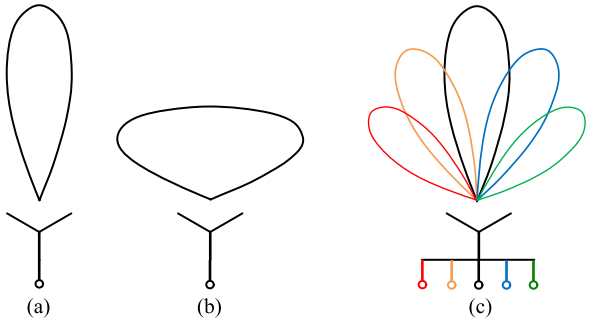

Fig. 1. Three design schemes of harvesting wireless RF power. (a) Narrow beam and high gain. (b) Wide beam and low gain. (c) Multiport and multibeam.

According to these studies, it can be found that converting and exploiting low RF power is still difficult for circuits. To confirm a higher level of harvested power, other ambient sources such as solar power [6], [36] and mechanical vibration [37], [38] were introduced into rectennas. Hybrid power harvesting feeds more power into a rectifier and can enhance power conversion efficiency [37], [38]. Without other ambient power, the rectenna efficiency could be less than satisfactory if the antenna fails to receive sufficient power under a low power density. Facing the restriction, it is an essential way of enabling the antenna to gather enough RF power into the circuit.

High-gain antennas, such as frequently used Yagi–Uda antennas [7], [39], [40] and patch antenna arrays [41]–[45] in rectenna designs can directly satisfy the requirement. Accumulating RF power in frequency domain has been widely reported [5], [7]–[10], [24], [27], [28], [35], [36], [40]. Multiple discrete antennas working at different frequencies were situated in one harvester [9]. Various broadband [5], [8], [24], [35], dual-band [7], [36], [40], and multiband [10], [27], [28] rectenna designs were proposed. The antenna polarization was also considered. Antennas with circular [6], [24], [43], [44], dual-linear [8], dual-circular [27], and all polarizations [46], [47] were used to reduce the loss caused by polarization mismatch.

Nevertheless, there are only several pieces of literature committing to effectively exploiting the incident RF waves from different directions. Adopting wide-beam antennas is a common way [4], [5], [8], [10], [27], [28], [35], [36], but inevitably leads to a low gain and a low level of sensitivity to the low power density. An array of the patch antenna with an enhanced beamwidth and compromised gain is presented [45]. With one antenna port, the gain and the beamwidth always conflict, which means one antenna port cannot receive the potentially high power at different angles. Multiple ports could exploit the potential of the antenna aperture since each port can be assigned to excite one beam that focuses on one direction. If the ports are well isolated, this type of antenna could be equivalent to multiple antennas of different high-gain beams. Thus, the multiport and multibeam antenna could be a promising solution. As illustrated in Fig. 1, it can realize wide-angle coverage by combining multiple narrow beams, of which one is separately excited by a port, and then owns two merits of the wide-beam and the high-gain antennas. In this design scheme, dc combining is necessary to maintain multiple beams and form a wide synthesized beam. In more detail, it means that RF power from every port should be individually converted by one of multiple rectifying branches and the rectified power be then combined.

Lately, a limited amount of the related research was presented [48]–[50]. In the rectenna design based on a 3-D-printed cuboid structure, two discrete patch antennas were adopted to harvest power from different directions [48]. This kind of conformal or nonplanar array can easily produce multiple beams and realize wide-angle coverage since it directly distributes the available antenna aperture to different directions of interest. The planar array concentrates more aperture to one direction. With the same geometric area, the planar array could have a larger gain and, hence, be more effective in the broadside direction. To enable the planar antenna array to collect power in a wide angle range, the beamforming technique was performed with two approaches, which were, respectively, based on Butler matrix and two hybrid couplers, and consequently, the gain and beamwidth were balanced [49], [50]. However, the extra beamforming network inevitably causes additional loss. If it can be integrated in the antenna or the antenna itself can produce multiple beams, the rectenna could be more compact and with less power loss.

In this paper, a grid-array antenna (GAA) without any extra beamforming networks is proposed to realize the purpose. Benefited from the capability of tilting the beam angle, two isolated ports at two opposite edges of GAA can excite two beams. It is also capable of being high gain. Furthermore, its simple structure is easy to fabricate and implement, and hence, extensively studied in millimeter-wave applications [52]–[56]. To easily integrate and to avoid more RF loss, coplanar striplines (CPS) are initially adopted to feed the GAA in this paper. A two-branch rectifier circuit with an RF balanced characteristic is introduced to combine the rectified dc power. Then, the proposed rectenna achieves a wider angle range for harvesting RF energy when compared to the grid-array rectenna used parasitic strips [51]. If the asymmetric rectifier circuit in the work [51] was replaced by this balanced one, there would be an improvement in the efficiency and stability. At 2.45 GHz, the measurement of the corresponding prototype demonstrates that the level of dc power can be more than 100 μW within an incident angle range of 59°, and the maximum efficiency is more than 45% under a power density of 1 μW/cm^2. In addition, the beamwidth of the rectenna is enhanced in a range from 2.37 to 2.45 GHz.

This paper is organized as follows. Section II analyzes the two-port GAA from aspects of the isolation, beam angle, and gain, and presents the design procedure to excite two independent high-gain tilted beams. Section III presents a compatible and CPS-based two-branch rectifier, which realizes effective rectification and dc power combining by using an RF balanced configuration and optimizing the matching impedance in an angle range. In Section IV, the validity of the design is proven by the measured results. In the final section, Section V, a conclusion will be made.

II. Investigation on GAA

The GAA is composed of grid meshes and a conducting plane, as shown in Fig. 2. Because of its simple structure,

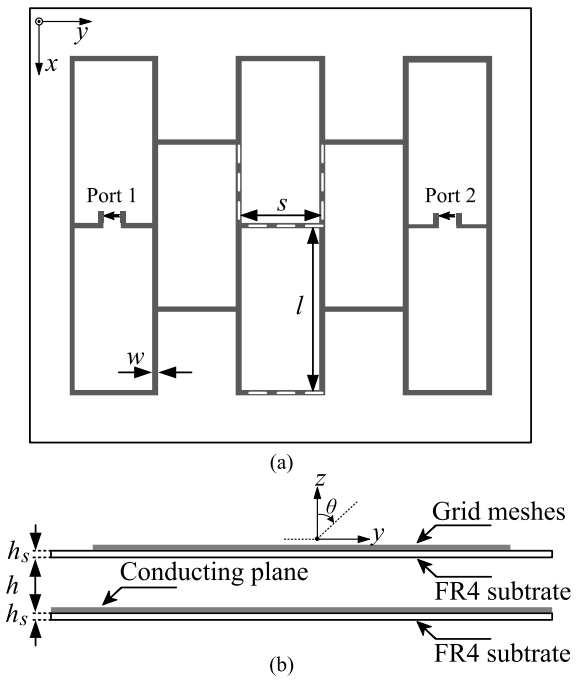

Fig. 2. Structure of the two-port GAA fed by CPS: (a) top view and (b) side view. It is the antenna part of the rectenna. Two substrates are with the same thickness of 1 mm, and the width of the grid lines w is 3 mm. θ, the polar angle of the spherical coordinate, indicates the incident direction of RF power. θ is positive in the right quadrants and negative in the left quadrants.

three key parameters are concerned in the design procedure: a height of grid meshes above the conducting plane ($h_s + h$), and two lengths of long (l) and short sides (s) of grid meshes. For the convenience of fabrication, GAA is designed on low-cost FR4 substrates with a relative dielectric constant of 4.4. To achieve better integration with the rectifier and reduce RF loss in matching network, CPS-based feeding is adopted, instead of coaxial feeding commonly employed in previous designs.

There are two types of GAA. One is designed to merely radiate broadside and the other one is with a steerable beam that scans with frequency (frequency-scanning beam). The former type owns a short side of $\lambda/2$ and a long side of λ for each grid mesh (λ is the wavelength). Because of the lengths, currents on the short sides would be in phase and radiate while currents on each long side would be out of phase and not radiate. Thus the antenna polarization follows the direction of short sides (y-direction). Though the mesh size of the latter type could change, it can be derived from the former type, and the main polarization remains y-direction. The former type that usually has a low profile was preferred in the recent research of millimeter-wave communication and radar applications [52]–[55]. In contrast, few studies in these years exploited the capability of steering or tilting the beam, with which GAA was initially proposed [57], [58]. The capability could make wireless power transfer (WPT) or harvest more stable since it makes the rectenna more adaptive to incident RF power from different directions. In the WPT system [56], though broadside GAA designs were considered and employed, a beam-steerable GAA was adopted as a transmitting antenna. However, the beam was steered by changing the polarities of GAA ports, not by utilizing the intrinsic capability of tilting the beam angle.

Besides the capability of tilting the beam angle, the traveling-wave characteristic of GAA merits considerable attention in this paper. By taking advantage of it and feeding GAA at two opposite ends along the traveling direction, two independent, high-gain, and symmetrically tilted beams are presented. Then, effectively harvesting RF energy in a wide angle range is realized.

To this end, three key parameters of GAA should be optimized in three aspects: the isolation, tilted angle, and gain. Good isolation between two ports guarantees that RF power could be collected independently by two tilted beams; an appropriate tilted beam angle could afford a wider range of the harvesting angle; a high gain ensures a high harvesting efficiency under a low power density.

These three parameters, the height and lengths of two mesh sides, will be systematically analyzed as follows. In the analysis, only port 1 is excited. Then, ports 1 and 2 are, respectively, excited to present the potential beamwidth improvement in the design example.

A. Height Above Conducting Plane

The analysis of the GAA height was made with regard to the gain, bandwidth, beamwidth, and resonant frequency [52]. Note that it is for the resonant and broadside case, where the ratio of long to short sides of meshes is always 2:1. In this section, the height is analyzed for a different case, where the GAA is dedicated to radiating with tilted beams.

A GAA can radiate backward and forward as the frequency increases. When a tilted beam is desired at a given frequency, the angle is preferred to be backward. In this case, the ratio of long to short lengths of grid meshes can be larger, so that the area occupied by GAA can be less. Hence, this type of GAA is considered for energy harvesting in this paper. In the design of the backward angle-fire GAA [57], it is mentioned that the ratio of its long to short sides can vary from 2:1 to 3:1. To demonstrate the role of the height of GAA, the long and short sides of GAA are with lengths of 127.2 and 42.4 mm (the ratio is 3:1).

An excessively small height could deteriorate radiation efficiency since the radiation elements, short sides of meshes, are parallel to the conducting plane. The height of broadside GAA designs are from $\lambda_0/33$ to $\lambda_0/10$ with substrates of $\varepsilon_r = 3$–7.3 [52]–[56]. With substrates of $\varepsilon_r = 1$, the heights of frequency-scanning [59] and backward angle-fire [57] GAA are around $\lambda_0/20$ and $\lambda_0/10$. The height could also be $\lambda_0/4$ as mentioned in [58]. As for the GAA in this paper, the major filling between the grid meshes and the conducting plane is air. Thus, heights of $\lambda_0/20$, $\lambda_0/10$, and $\lambda_0/4$ are selected as representative values to be investigated.

The height has a small impact on the gain and beamwidth. It is found that the height is the main factor that affects the isolation between two ports. As illustrated in Fig. 3, the isolation becomes worse when the height is smaller. This is because the grid meshes getting closer to the conducting plane, the short sides behave more like transmission lines but

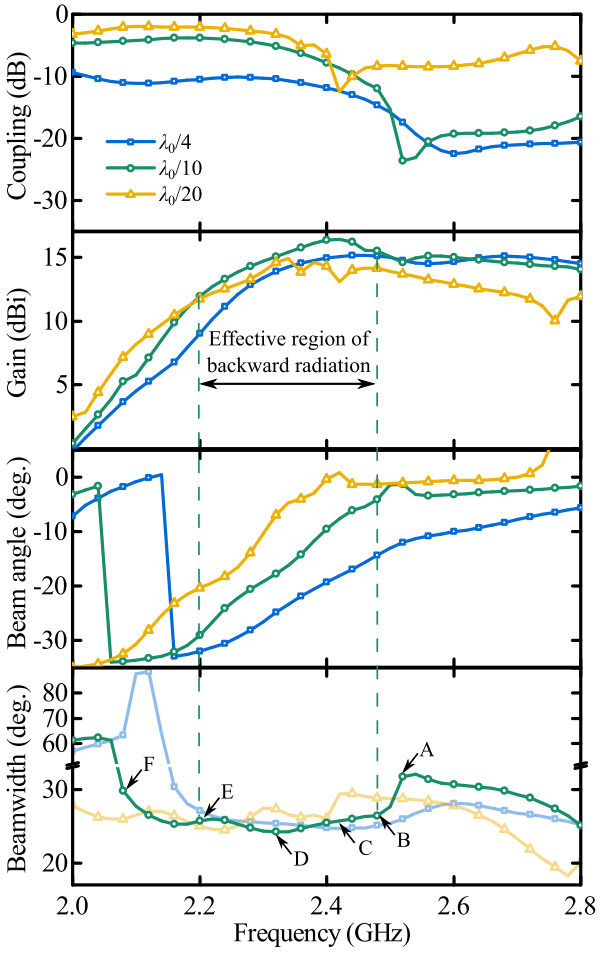

Fig. 3. Simulated coupling, maximum y-polarized gain of yoz plane, beam angle, and the beamwidth for different heights. The gain, beam angle, and beamwidth are obtained by only exciting port 1. The curve of coupling is the upper bound, since it is obtained on the condition that two ports are matched at every simulated frequency. Points A–F are marked on the beamwidth curve of $\lambda/10$ to illuminate the effective frequency region of backward radiation.

less as radiating elements, and the RF power attenuates more slowly. On the other hand, from the results of the gain and beam angle, it can be deduced that a small height, though permits a low profile, restricts the beam angle of the high gain to the broadside and then leads to a low efficiency in harvesting incident RF power coming from other directions.

B. Long and Short Lengths of Grid Meshes

Lengths of sides of grid meshes account for the operating frequency and tilted angles. The GAA for energy harvesting is expected to radiate with backward beams. Thus, the effective frequency region of backward radiation where the GAA owns backward beam angles and high gains is first defined in this section. In Fig. 3, with respect to the case of $\lambda_0/10$, the backward angle-fire region is between point A and F. In the region between point B and D, the beam angle and beamwidth are stably declining, the gain is relatively high and the peak gain occurs at point C. From point B to A, the beamwidth abruptly rises, the beam angle approaches 0° and the gain decreases. It is due to the resonance phenomenon as demonstrated by the current distribution shown in Fig. 4.

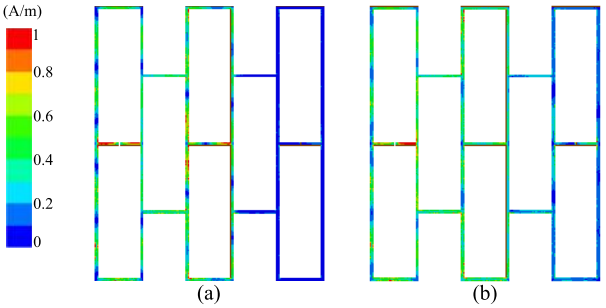

Fig. 4. Surface current distribution of (a) point A and (b) point B in Fig. 3 when only port 1 is excited. The current of point B is distributed on all of grid meshes and attenuates along the traveling direction. On the contrary, the current distribution of point A is confined to the left part, where the current appears not to attenuate due to the resonance.

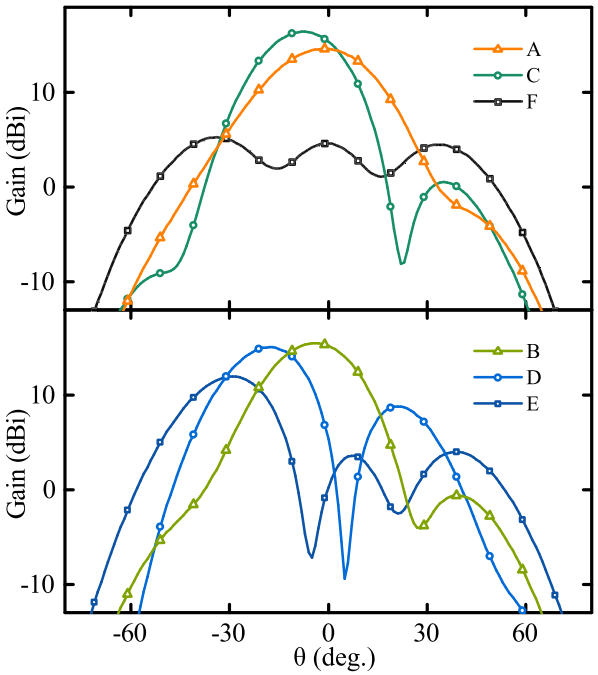

Fig. 5. Antenna patterns in yoz plane of points A–F marked in Fig. 3 when only port 1 is excited. A and F are outside the effective region of backward radiation, and C has the peak gain. The gradient of the beamwidth varies at B, D, and E.

The gradient of the beamwidth curve varies at points D and E, which indicates the being of the first and second obvious side lobes, respectively. From point E, the gain rapidly deteriorates and the magnitude of the two side lobes becomes closer to that of the main lobe. The beam is abruptly enlarged at point F. The corresponding patterns are depicted in Fig. 5. Therefore, the effective region of backward radiation is defined as between the points B and E.

It is known that long and short lengths have a marked impact on the beam angle. The relationship can be explained by using the following equation [58]:

$$\sin\theta = \frac{l/s}{p_x} + \frac{1}{p_y} - \frac{\lambda}{s} \tag{1}$$

where θ is the beam angle as shown in Fig. 2, and p_x and p_y are the relative phase velocities along long and short sides.

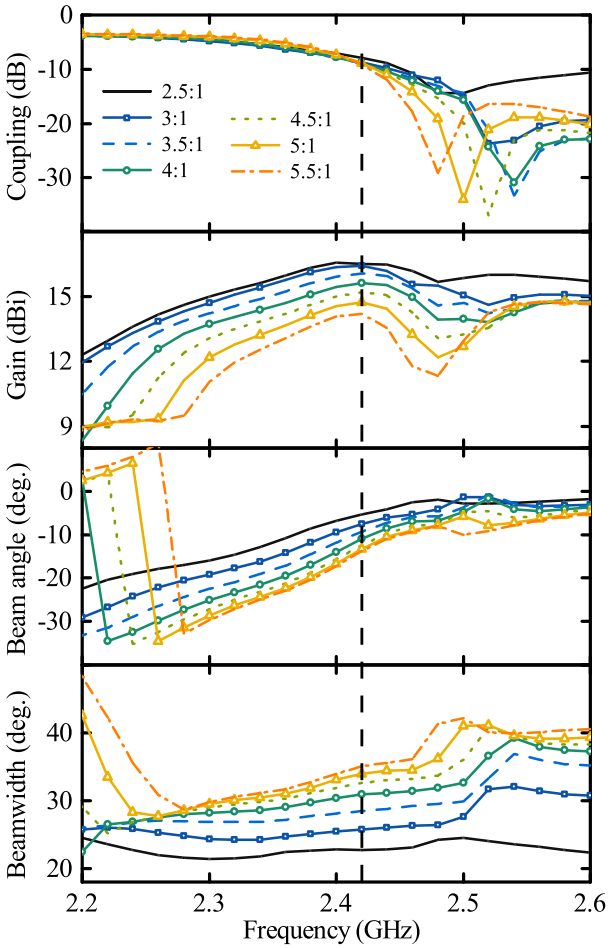

Fig. 6. Simulated upper bound of coupling, maximum y-polarized gain of yoz plane, beam angle, and beamwidth for different ratios of long to short sides. The gain, beam angle, and beamwidth are obtained by only exciting port 1. The vertical dashed line marks the frequency that has peak antenna gains of different ratios.

The beam angle varies with two factors, l/s and s/λ. One is the ratio of long to short sides and the other one reflects the influence of the frequency. However, very few studies elaborate on how to make GAA operate with a desired tilted beam angle in the effective region of backward radiation, especially with respect to the application of GAA in this paper. To clearly illustrate that, several cases adopted the same height ($\lambda_0/10$) and the same sum of lengths of long and short sides (or the same perimeter of grid meshes) but different ratios of long to short sides are presented with simulated results of the antenna gain, tilted angle, and beamwidth, as shown in Fig. 6.

Fig. 6 clearly indicates that the same perimeter results in the occurrence of the peak gain at the same frequency that is close to the upper limit of the effective region of backward radiation; different ratios make the bandwidth of the effective region of backward radiation, beamwidth, and beam angle different. A large ratio brings a large tilted beam angle and a little decrease of the antenna gain since the antenna aperture shrinks. However, when the perimeter is kept unchanged, a limit of the beam angle exists. Assuming that the perimeter, or $l + s$, is constant in (1), a large value of l leads to a small value of s, and the contribution of the ratio (l/s) increase could be

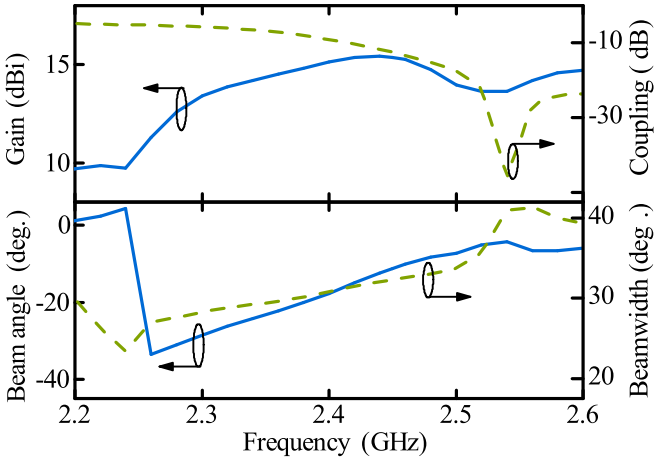

Fig. 7. Simulated upper bound of coupling, maximum y-polarized gain of yoz plane, beam angle, and beamwidth for the adopted GAA. Only port 1 is excited.

canceled by the term of λ/s. In Fig. 6, a threshold for the beam angle appears when the ratio is about 5:1. From this threshold value, the beam angle will not obviously increase. In addition, the effective region of backward radiation also obviously decreases and the gain deteriorates.

It is noteworthy that the effective region of backward radiation could fail to effectively harvest RF power if the antenna ports have strong coupling. The coupling could decrease the received power and deteriorate the rectenna performance. Thus, the operating region for harvesting applications should be in the effective region of backward radiation and with weak coupling or good isolation between antenna ports.

C. Adopted Design

According to the investigation mentioned-above, the design procedure can be carried out in this way.

1) Choose a minimum value of the height to meet the isolation requirement ($\geqslant$10 dB).
2) Choose a proper perimeter of grid meshes, to ensure that the backward angle-fire GAA is with a peak gain at an expected frequency.
3) Elevate the ratio of lengths if the tilted angle is not large enough; reduce it otherwise.
4) If the beam angle of the peak gain cannot be further backward by increasing the ratio, and a lower frequency in the operating region can meet the demands on the beam angle and the gain, reduce the perimeter of grid meshes to shift the operating region.
5) If the performance of the operating region is not adequate, try to elevate the height.

In the design example, the adopted height is 15 mm, which is $\lambda/8.16$ larger than $\lambda/10$; hence, it can provide better isolation, as shown in Fig. 7. The width of grid lines is 3 mm, and the long and short lengths of grid meshes are 137 and 32.6 mm. A comparison of GAA configurations is presented in Table I. It can be found that a ratio of 4.2:1, which is higher than those adopted in previous GAA designs, is selected to serve the RF energy harvesting, and results in a smaller occupied area. In consequence, the peak y-polarized gain occurs at 2.45 GHz, where the beam excited by port 1 or

TABLE I
COMPARISON WITH COMMON GRID-ARRAY CONFIGURATIONS

Type	Profile	Short side s	Ratio l/s	Feeding
Broadside	$(1/33–1/10)\lambda_0$	$\lambda_g/2$	2:1	Coaxial
Backward*	$\lambda_0/10$	$\geqslant\lambda_g/3$	$>$2:1 & $\leqslant$3:1	Coaxial
This Work	$\lambda_0/8.16$	$\lambda_g/3.5$	4.2:1	CPS

*It refers to the specific design for radiating with a backward angle-fire beam [57]. Grid-array antennas with heights of $\lambda_0/4$ [58] and $\lambda_0/20$ [59] put emphasis on the frequency-scanning property and not optimized for radiating backward, thus not included.

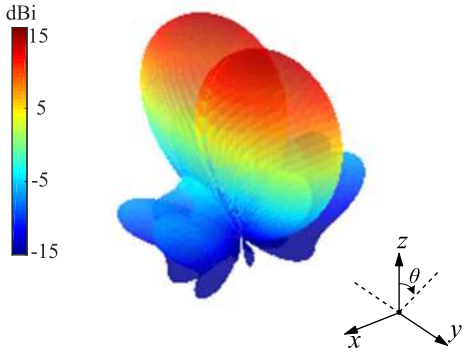

Fig. 8. Illustration of two overlapped beams of the adopted GAA at 2.45 GHz. The two beams are excited by ports 1 and 2, respectively.

2 is with an angle of $\pm 13°$. Assuming the power density is 1 μW/cm^2, the RF power received by GAA can be calculated by

$$P_r = D \cdot \frac{G_r \lambda^2}{4\pi} \tag{2}$$

where D is the power density, G_r is the gain of the receiving antenna, and λ is the wavelength.

Thus, a 6.5- and 10-dBi gain can afford -12.7- and -9.2-dBm RF power at 2.45 GHz, with which the efficiency of rectification could approach 30% and 40%, respectively, according to the state of the art [11]. Two beams excited by two ports are symmetrically tilted in *yoz* plane and can largely enhance the high-gain beamwidth, as illustrated in Fig. 8. To demonstrate the performance of the two-beam GAA, the synthesized patterns are depicted in Fig. 9. Since the rectenna design combines rectified dc power instead of RF power, the synthesized patterns of the antenna are obtained by adding up the magnitudes of two beams excited by two ports, respectively, without regard to the relative phase of two beams. It can be seen that the pattern begins to merge at higher frequencies while split at lower frequencies, and a wide beamwidth can be maintained in a frequency band. The 2.45-GHz synthesized pattern is wide beam and also high gain. At 2.45 GHz, the maximum gain of one individual beam is up to 15.5 dBi and the synthesized beamwidths of 10- and 6.5-dBi gains are extended to 74° and 90°, respectively, which permits high sensitivity to low power density in a wide-angle range. Meanwhile, the simulated isolation of 2.45 GHz is more than 12.4 dB. Since the terminal impedances of the two-port GAA (input impedances of the rectifier) vary with the input power,

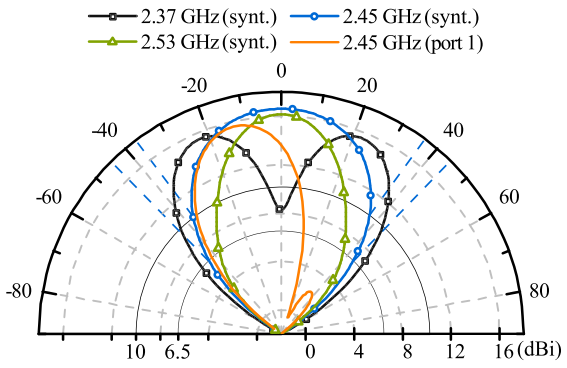

Fig. 9. Simulated radiation patterns of the adopted GAA design in *yoz* plane, including synthesized beams that are sum of gain magnitudes, and a 2.45-GHz beam of port 1.

and two beams are symmetric and overlapped around 0°, two ports could be simultaneously well matched only at angles around 0°. At these angles, the coupling would approach the simulated maximum, as presented in Fig. 7, results in the worst isolation level. However, the overlapped range is small and the isolation could be better elsewhere.

The isolation also makes it simple to simulate and optimize the rectifying circuit since two branches of rectifier can be approximately simulated with no coupling.

III. RECTIFYING CIRCUIT AND MATCHING APPROACH

Two differently tilted beams excited by two ports are utilized to broaden the angle coverage of receiving RF power. Thus, the RF power received by two ports needs to be converted, respectively, to dc power. Then, the dc power is combined and fed into a load. With the demand, a rectifier with two rectifying branches is considered.

To obtain a stable design, the RF part of the rectenna, including the rectifying circuits and GAA, is designed on one plane, and pins are used for dc connection, and dc lines are separated by a conducting plane, as shown in Fig. 10. It ensures the antenna performance free from the interference of dc lines.

A. Topology of Rectifying Circuit

Rectified dc power usually needs to be further processed by a power management module (PMM), which includes a dc–dc converter to elevate the low voltage to a usable level. Each branch could be followed by one PMM so that rectified dc power can be first processed by PMM and then combined. To reduce the cost and the design complexity, two branches are expected to share one PMM in this paper. In this way, the rectified dc power is first combined and then delivered to a PMM, which is represented by a resistive load in the following analysis.

Configurations of the latter method prefer a voltage doubler that is composed of a series and a shunt diodes in each branch of the rectifier [8], [10], [24], [27], [28]. However, it could not be a good choice for a system of the balanced transmission line like CPS in this paper. To demonstrate it, four rectifier configurations A, B, C, and D, respectively, using one shunt diode, one series diode, two series diodes, and a voltage

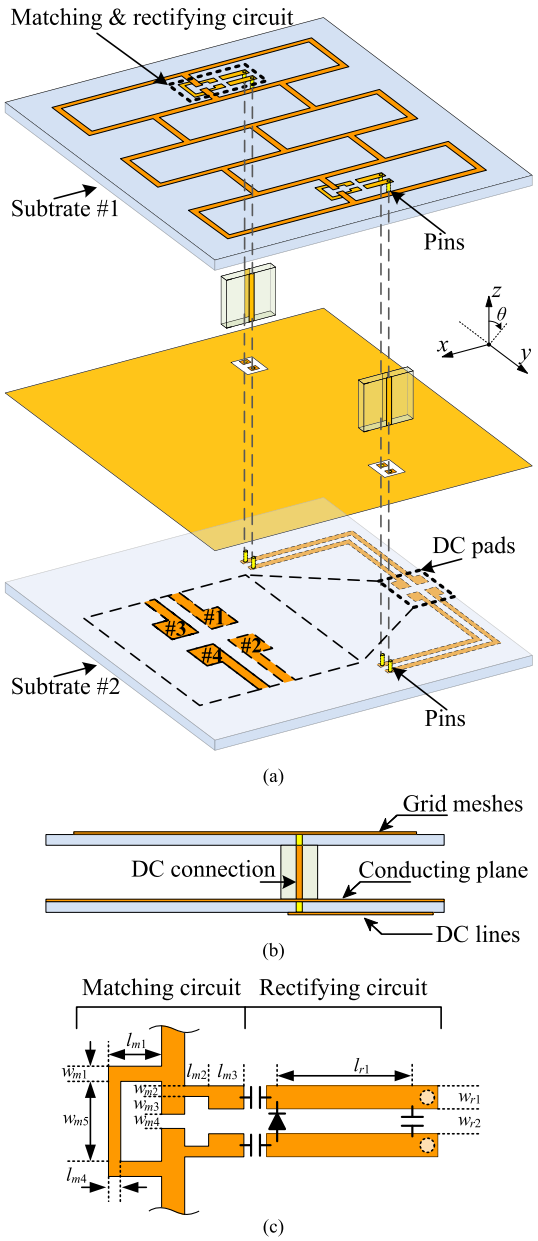

Fig. 10. Detailed structure of the rectenna. (a) Isometric view. (b) Side view. (c) Matching and rectifying circuit. In (a), four dc pads are designed for testing every branch individually, evaluating the combining effect, and also conveniently debugging each rectifying branch. In (c), $w_{m1} = 1$ mm, $w_{m2} = 0.8$ mm, $w_{m3} = 1.2$ mm, $w_{m4} = 1.2$ mm, $w_{m5} = 5.2$ mm, $l_{m1} = 5.1$ mm, $l_{m2} = 2$ mm, $l_{m3} = 3.1$ mm, $l_{m4} = 1$ mm, $w_{r1} = 2.1$ mm, $w_{r2} = 1$ mm, and $l_{r1} = 19.6$ mm.

doubler in each rectifying branch as shown in Fig. 11, are compared. The four configurations are all based on CPS and twin-wire dc lines of the same length. Since the symmetry of the antenna and its two tilted beams, two branches of one rectifier configuration and their source impedances (Z_s) are the same. In one branch of the rectifier circuit, one or two Schottky diodes SMS7630 are used for converting RF to dc power, two series capacitors for blocking the generated dc component, and one shunt capacitor for blocking RF components. To form a close dc path in simulation, an ideal RF block, or named ideal dc feed, is used in configuration B and C. To approach their highest efficiencies, the dc loads of four configurations are different because of the different numbers of diodes. R_{L1} is 3000 Ω, for configuration A and B, while R_{L2} is 6000 Ω, for configuration C and D.

The simulated results of RF-to-dc conversion efficiency are depicted in Fig. 12. Since main lobes of two antenna beams are overlapped with high gains around 0°, and not overlapped elsewhere, the levels of input RF power of two rectifying branches could be equal or very different. To evaluate these configurations, the input RF power of one rectifying branch P_{in1} is assigned to be −10 dBm, and P_{in2} for the other branch varies from −30 to 10 dBm in the simulation. The point where P_{in2} is −10 dBm represents the overlapped situation, and the regime where P_{in2} is far less than −10 dBm represents the other situation. To fairly compare these four configurations, they are, respectively, matched at the point where P_{in2} is equal to −10 dBm.

Whatever the number of diodes is, the balanced configurations, A and C, always provide obvious superiority over unbalanced ones, B and D. The sharp efficiency decrease in B and D is due to the common mode inspired by the asymmetric rectifying circuits. In the balanced transmission lines, the RF power of the common mode that cannot be blocked by the bypass capacitor probably radiates and leaks to the dc lines and the load. Consequently, it could make the dc output unstable when dealing with dc power and lead to the efficiency loss. To avoid the loss caused by the common mode and improve the efficiencies of B and D, the balanced CPS can be replaced by unbalanced transmission lines (like microstrip lines) for rectifying circuits. It usually needs a balun as a transition. Though this improvement could make the efficiencies of B and D close to A and C, the transition will lead to an additional loss and design complexity. Thus, the symmetric rectifying circuits in A and C are better for the balanced transmission lines. When comparing configurations A and C, fewer diodes also bring less loss.

To pursue a high efficiency, configuration A is adopted.

B. Optimization of Matching Impedance

The impedance of the rectifying circuit varies with the input RF power. Since the amount of received RF power changes with the beam angle of the antenna, impedance matching should be optimized in an angle range for this design, rather than at one angle.

Assuming that the power density is 1 μW/cm^2, the received RF power separately fed into two branches of the rectifier is calculated from the antenna gains by using (2). By putting the evaluated value of RF power into P_{in1} and P_{in2} in the simulation of configuration A, and sweeping the imaginary and real parts of the source impedance Z_s, simulated contours of constant values of $P_{t,\text{dc}}$ are presented in Fig. 13, where the $P_{t,\text{dc}}$ is the sum of output dc power of both two branches at every degree in the concerned angle range (−100°–100°), and can be expressed as

$$P_{t,\text{dc}} = \sum_{i=-100}^{100} P_{i,\text{dc}} \tag{3}$$

$$P_{i,\text{dc}} = V_{i,\text{dc}}^2 / R_{L1} \tag{4}$$

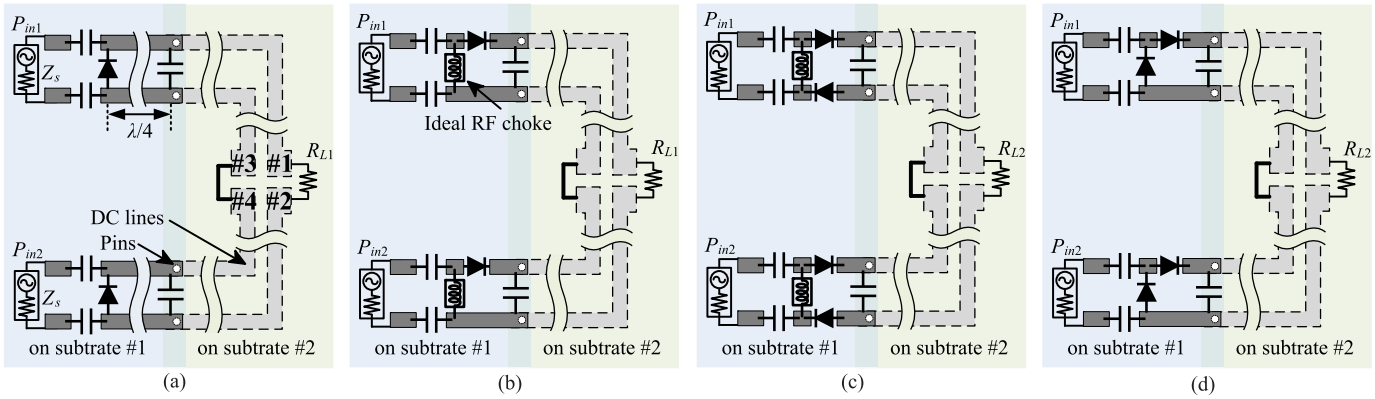

Fig. 11. Configurations of four rectifiers A–D and all based on the same structure in Fig. 10. A is adopted.

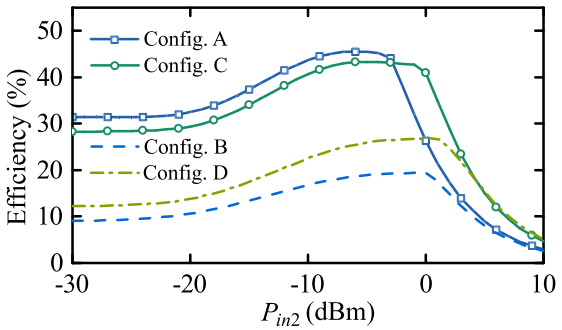

Fig. 12. Simulated RF-to-dc conversion efficiencies of configurations in Fig. 8. The efficiencies include return loss. $P_{\text{in}}1$ is always -10 dBm. Four configurations, respectively, matched at the point where $P_{\text{in}}2$ is equal to -10 dBm.

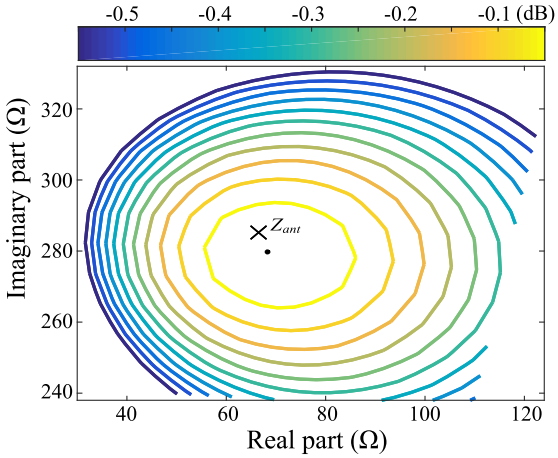

Fig. 13. Contour lines of normalized sum of rectified power of every angle ($P_{t,\text{dc}}$), which varies with the real and imaginary parts of the source impedance Z_s of the adopted rectifier (configuration A). One decrement is 0.05 dB. The inner point is 0 dB. The impedance of the marked point equals Z_{ant}.

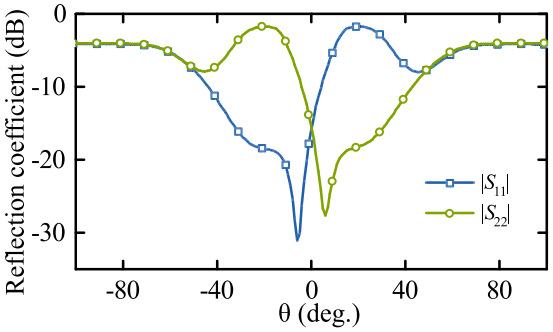

Fig. 14. Reflection coefficients of the adopted rectifier when adopting the impedance Z_{ant} as the source impedance Z_s at 2.45 GHz. The magnitudes $|S_{11}|$ and $|S_{22}|$ reflect the matching condition or the return loss of two rectifying branches, respectively, connected to ports 1 and 2.

where $P_{t,\text{dc}}$ indicates the overall performance of the rectenna, i indicates the degree of the beam angle, $V_{i,\text{dc}}$ is the dc voltage on the load, $P_{i,\text{dc}}$ is the dc power, and R_{L1} is the load resistance.

It reveals the optimum range of the matching impedance for each rectifying branch. Based on the simulation results, a compact matching circuit, composed of a short stub and a piece of a stepped-impedance line, is proposed between GAA and the rectifying circuit as shown in Fig. 10. With the matching circuit, the input impedance of the antenna, simulated at 2.45 GHz, is marked as Z_{ant} in Fig. 13.

After Z_{ant} is assigned to Z_s, rectifier parameters, including return loss, combined output dc power, and RF-to-dc conversion efficiency with respect to the beam angle, are simulated to interpret the validity of the matching impedance optimization.

When comparing Figs. 14 and 9, it can be found that each rectifying branch is well matched (reflection coefficient $\leqslant -10$ dB) when the antenna gain is more than 6 dBi (equally -13.2 dBm at 1 μW/cm^2) for an individual beam. It can be found that two branches are well matched to their corresponding antenna ports in the angle range of its own main lobe. In a part of each other's main lobe, two branches are mismatched. Since the corresponding gain and received power are small, the power loss can be neglected, and the isolation between two branches can be better. The -10-dB width is 44° for each beam and totally 86° for the synthesized beam. As a consequence, a wide-angle range of the beam can be utilized. The results shown in Fig. 15 illustrate that relatively flat curves of both the dc output and the overall efficiency are achieved in a wide-angle range at 2.45 GHz. The maximum dc power is -6.6 dBm and the corresponding RF-to-dc conversion efficiency is 48%, which is calculated by

$$\eta_i = \frac{P_{i,\text{dc}}}{D(G_{i,r1} + G_{i,r2})\lambda^2/(4\pi)} \tag{5}$$

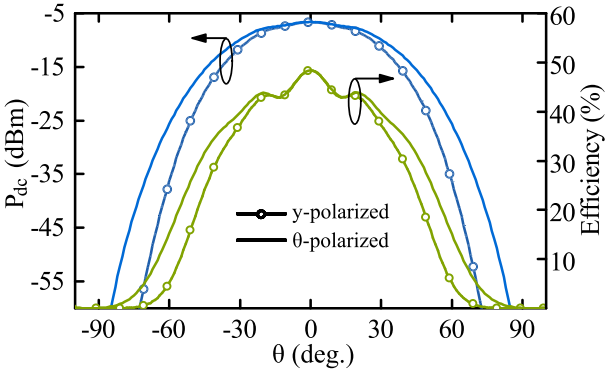

Fig. 15. Simulated output dc power and RF-to-dc conversion efficiencies of the adopted rectifier at 2.45 GHz.

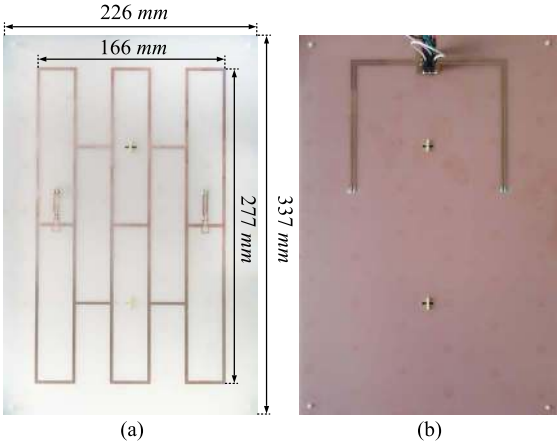

Fig. 16. Fabricated rectenna. (a) Top view. (b) Bottom view.

where i indicates the degree of the beam angle, $P_{i,\mathrm{dc}}$ is the dc power on the resistive load, and $G_{i,r1}$ and $G_{i,r2}$ are the gains of two beams.

IV. Measurements of Grid-Array Rectenna

On the basis of detailed investigations presented in Sections II and III, a prototype shown in Fig. 10 is fabricated and measured as shown in Figs. 16 and 17. A linearly polarized antenna is used to transmit the RF power, and the rectenna under test rotates in its yoz plane. The measured results of the dc output are directly presented with the θ polarization, of which the antenna pattern is close to the y-polarized pattern since the z-polarized contribution is relatively weak as illustrated in Fig. 15.

A. Effect of Combining dc Power

To verify the effect of combining dc power, the dc voltages produced by one branch and combined from two branches are tested, respectively.

For this purpose, four dc pads are designed. When measuring the performance of the combined output, two pads in different branches are connected with a resistor while the other two pads are shorted as shown in Fig. 18(a). In the other case, every branch is measured on the condition that every two pads of one branch are connected with a resistor, as shown by the diagram in Fig. 18(b).

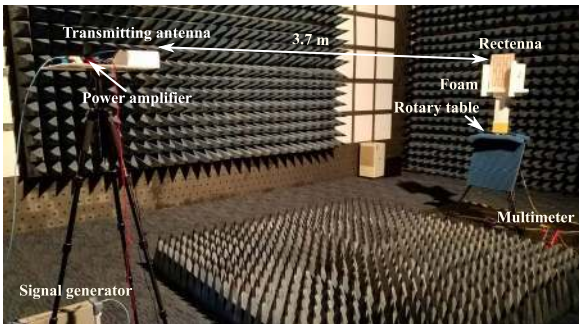

Fig. 17. Photograph of the measurement setup. The rotary table and the multimeter were controlled by a computer. The power density was confirmed by a linearly polarized antenna, of which the gain is 4.8 dBi at 2.45 GHz.

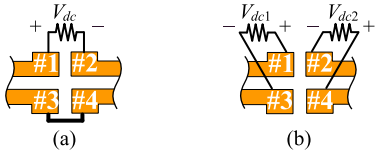

Fig. 18. Connection diagrams of two measured cases. (a) Combining dc output from two branches. (b) Leaving outputs of two branches separate. The resistance of all resistors is R_{L1} (3 kΩ).

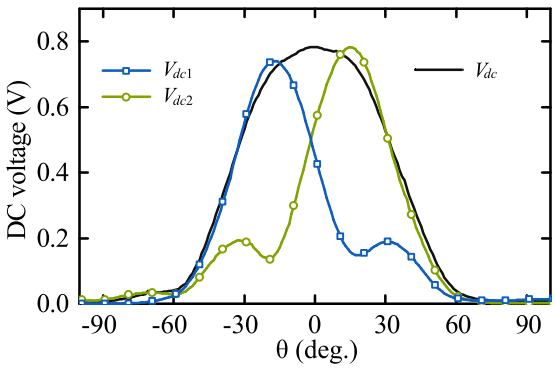

Fig. 19. Performance of combining dc power from two branches at 2.45 GHz.

Fig. 19 presents the measured output dc voltages. It validates that the adopted rectifier can effectively combine dc power. The angle range of 0.5-V dc output (83.3 μW) is doubled, and the combined result almost covers both results of V_{dc1} and V_{dc2}, so that an extended angle range of harvesting is permitted.

B. Overall Performance at Frequencies

The rectenna is measured with a power density of 1 μW/cm^2 in a frequency band from 2.39 to 2.47 GHz. The corresponding results are shown in Fig. 20. The measured result of 2.45 GHz is close to the simulation. A small decrease in the level of the dc output power in the whole angle range is probably due to a slight mismatch.

The results show a high performance between 2.39 and 2.45 GHz. In the measurement of 2.45 GHz, the maximum dc output power is more than 200 μW and the maximum RF-to-dc efficiency is calculated to be 45.3%. And the angle range can reach 96° if the dc power is desired to be more

TABLE II

PARAMETERS OF HIGH-GAIN RECTENNAS FOR LOW POWER DENSITIES AT FREQUENCIES AROUND 2.45 GHz

Reference	Freq. (GHz)	Substrate	Antenna size (cm^2)	No. of Beam-s	Beamforming network	Max. gain [a] (dBi)	Antenna aperture efficiency (%)	RF power density ($\mu W/cm^2$)	η_{RF-dc} (%)	P_{dc} (μW)	EPD [b] ($\mu W/cm^2$)
Yagi [39]	2.45	None	5.75×15.9	1	\	11.8	197.53	1	∼53.4	96.4	1.0544
Yagi [40]	2.45	RO3850	5.646×6.15	1	\	7.59	197.28	1	∼51.3	35.5	1.0224
Yagi array [7]	2.14	RT5880	∼10×39	1	\	∼13.3	85.73	0.0455	∼34	∼5.2	0.0133
Patch array [49]	2.52	RO4003	NA×28	4	Butler matrix	9.6	NA	0.04	14	0.519	NA
Patch array [50]	2.45	FR4	10×24	4	Butler matrix	9.7	46.4	NA	NA	100	0.4167
				2	Hybrid coupler	8.7	36.85	NA	NA	95.5	0.3979
This work	2.45	FR4	22.6×33.7	2	No need	15.5	55.59	1	45.3	203.8	0.2676
Grid array [c]			(16.6×27.7)			(14.6)	(74.84)	0.5	35.2	77.8	0.1022
								0.1	20.3	8.6	0.0113
								0.052	16.3	3.6	0.0047

[a] For multi-beam antennas, it is the maximum gain of the most high-gain beam; the antenna aperture efficiency is calculated from this maximum gain and the antenna size.
[b] EPD: the equivalent dc power density, is obtained by dividing the output dc power (P_{dc}) by the antenna size. It has a positive correlation with the antenna aperture efficiency, can be generally expressed by the product of the antenna aperture efficiency, the RF power density and the RF-to-dc conversion efficiency (η_{RF-dc}).
[c] A space exists between the substrate outline and grid meshes of the proposed rectenna. It is left for nylon crews that fix and support the substrates, and can be removed to increase the aperture efficiency and equivalent dc power density. The results of the trimmed GAA are given in brackets.

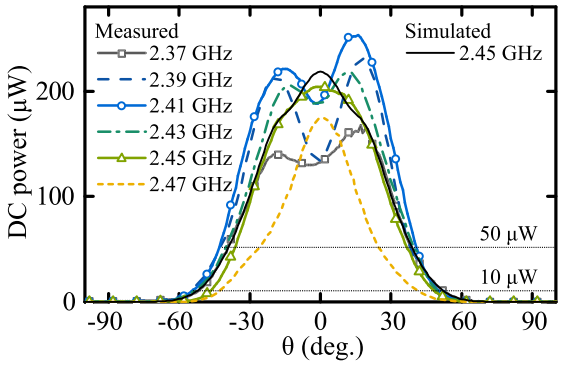

Fig. 20. Measured patterns of the rectenna from 2.37 to 2.47 GHz. The marked point is of the maximum efficiency.

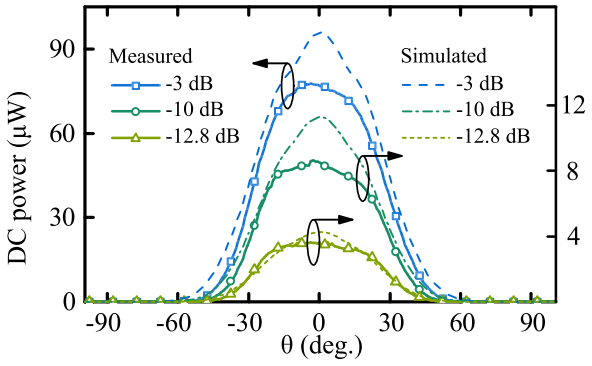

Fig. 21. Measured levels of the output dc power of 2.45 GHz at −3-, −10-, and −12.8-dB lower densities (0.5, 0.1, and 0.052 $\mu W/cm^2$).

than 10 μW. If elevating the threshold to 100 μW, it can reach 59°. Larger beam angles of lower frequencies result in wider beamwidths. The angle range of more than 100 μW is up to 74° at 2.41 GHz. The beam of the rectenna merges at higher frequencies from 2.47 GHz. The prototype keeps a wide range of relatively high dc output in a narrowband and, thus, can be applied for harvesting power in IEEE 802.11 b/g bands.

C. Measurements at Lower Power Densities

The density in the above-mentioned measurements is 1 $\mu W/cm^2$. However, it could be even lower in fact. To be closer to reality, cases with 3-, 10-, and 12.8-dB lower RF power densities (0.5, 0.1, and 0.052 $\mu W/cm^2$) were measured at 2.45 GHz. The measured results are shown in Fig. 21. The maximum efficiencies are 35.2%, 20.3%, and 16.3% for cases of 0.5, 0.1, and 0.052 $\mu W/cm^2$, and the maximum levels of dc power are 77.8, 8.6, and 3.6 μW. Under such low power densities, the rectenna still maintains a relatively wide beamwidth. If setting the thresholds of the dc output 25, 2.5, and 1 μW for 0.5, 0.1, and 0.052 $\mu W/cm^2$, respectively, the angle range can reach 68°. However, higher performance is possible according to the simulation. Since the coupling is not included in the rectifier simulation, the margin between the measured and simulated results around 0° could be reduced by further improving the isolation of two ports.

It can be concluded that the rectenna design is also effective for much lower densities. Note that the prototype was measured with a single-frequency source. If power from a frequency band is accumulated, it could be more capable. In Table II, this paper is compared with rectennas designed for low power densities around 2.45 GHz. Due to the endfire radiation of Yagi–Uda antennas, the aperture efficiency and the equivalent dc power density are calculated to be higher than designs with broadside beams including this paper grid-array rectenna. However, compared with broadside designs in [50], this paper has higher aperture efficiency. In view of the basic similarity in designs of [49], [50] and the positive correlation between the equivalent dc power density and the antenna aperture efficiency, it can be deduced from Table II that the proposed rectenna can provide competitive performance.

V. CONCLUSION

A possibility is presented that a simple configuration of the rectenna can achieve high sensitivity to low-density RF energy in a wide-angle range. The designed rectenna can be decomposed into two parts: a traveling-wave GAA affording

both the wide synthesized beamwidth and the high gain without any extra beamforming networks, and a balanced rectifier effectively combining dc power with one shunt diode in every branch. The simple structure permits easy implementation.

It could be an effective solution to the case that the source location is unclear or multiple sources exist at different places.

REFERENCES

[1] S. Gollakota, M. S. Reynolds, J. R. Smith, and D. J. Wetherall, "The emergence of RF-powered computing," *Computer*, vol. 47, no. 1, pp. 32–39, Jan. 2014.

[2] S. Kim *et al.*, "No battery required: Perpetual RFID-enabled wireless sensors for cognitive intelligence applications," *IEEE Microw. Mag.*, vol. 14, no. 5, pp. 66–77, Jul./Aug. 2013.

[3] S.-N. Daskalakis, J. Kimionis, A. Collado, G. Goussetis, M. M. Tentzeris, and A. Georgiadis, "Ambient backscatterers using FM broadcasting for low cost and low power wireless applications," *IEEE Trans. Microw. Theory Techn.*, vol. 65, no. 12, pp. 5251–5262, Dec. 2017.

[4] S. D. Assimonis, S.-N. Daskalakis, and A. Bletsas, "Sensitive and efficient RF harvesting supply for batteryless backscatter sensor networks," *IEEE Trans. Microw. Theory Techn.*, vol. 64, no. 4, pp. 1327–1338, Apr. 2016.

[5] R. J. Vyas, B. B. Cook, Y. Kawahara, and M. M. Tentzeris, "E-WEHP: A batteryless embedded sensor-platform wirelessly powered from ambient digital-TV signals," *IEEE Trans. Microw. Theory Techn.*, vol. 61, no. 6, pp. 2491–2505, Jun. 2013.

[6] J. Bito, R. Bahr, J. G. Hester, S. A. Nauroze, A. Georgiadis, and M. M. Tentzeris, "A novel solar and electromagnetic energy harvesting system with a 3-D printed package for energy efficient Internet-of-Things wireless sensors," *IEEE Trans. Microw. Theory Techn.*, vol. 65, no. 5, pp. 1831–1842, May 2017.

[7] H. Sun, Y.-X. Guo, M. He, and Z. Zhong, "A dual-band rectenna using broadband yagi antenna array for ambient RF power harvesting," *IEEE Antennas Wireless Propag. Lett.*, vol. 12, pp. 918–921, 2013.

[8] C. Song, Y. Huang, J. Zhou, J. Zhang, S. Yuan, and P. Carter, "A high-efficiency broadband rectenna for ambient wireless energy harvesting," *IEEE Trans. Antennas Propag.*, vol. 63, no. 8, pp. 3486–3495, Aug. 2015.

[9] M. Piñuela, P. D. Mitcheson, and S. Lucyszyn, "Ambient RF energy harvesting in urban and semi-urban environments," *IEEE Trans. Microw. Theory Techn.*, vol. 61, no. 7, pp. 2715–2726, Jul. 2013.

[10] V. Kuhn, C. Lahuec, F. Seguin, and C. Person, "A multi-band stacked RF energy harvester with RF-to-DC efficiency Up to 84%," *IEEE Trans. Microw. Theory Techn.*, vol. 63, no. 5, pp. 1768–1778, May 2015.

[11] S. Hemour *et al.*, "Towards low-power high-efficiency RF and microwave energy harvesting," *IEEE Trans. Microw. Theory Techn.*, vol. 62, no. 4, pp. 965–976, Apr. 2014.

[12] C. H. P. Lorenz *et al.*, "Breaking the efficiency barrier for ambient microwave power harvesting with heterojunction backward tunnel diodes," *IEEE Trans. Microw. Theory Techn.*, vol. 63, no. 12, pp. 4544–4555, Dec. 2015.

[13] E. Falkenstein, M. Roberg, and Z. Popovic, "Low-power wireless power delivery," *IEEE Trans. Microw. Theory Techn.*, vol. 60, no. 7, pp. 2277–2286, Jul. 2012.

[14] A. Collado and A. Georgiadis, "Optimal waveforms for efficient wireless power transmission," *IEEE Microw. Wireless Compon. Lett.*, vol. 24, no. 5, pp. 354–356, May 2014.

[15] C. R. Valenta, M. M. Morys, and G. D. Durgin, "Theoretical energy-conversion efficiency for energy-harvesting circuits under power-optimized waveform excitation," *IEEE Trans. Microw. Theory Techn.*, vol. 63, no. 5, pp. 1758–1767, May 2015.

[16] M. Roberg, T. Reveyrand, I. Ramos, E. A. Falkenstein, and Z. Popovic, "High-efficiency harmonically terminated diode and transistor rectifiers," *IEEE Trans. Microw. Theory Techn.*, vol. 60, no. 12, pp. 4043–4052, Dec. 2012.

[17] J. Guo, H. Zhang, and X. Zhu, "Theoretical analysis of RF-DC conversion efficiency for class-F rectifiers," *IEEE Trans. Microw. Theory Techn.*, vol. 62, no. 4, pp. 977–985, Apr. 2014.

[18] S. Abbasian and T. Johnson, "Power-efficiency characteristics of class-F and inverse class-F synchronous rectifiers," *IEEE Trans. Microw. Theory Techn.*, vol. 64, no. 12, pp. 4740–4751, Dec. 2016.

[19] Y. Huang, N. Shinohara, and T. Mitani, "A constant efficiency of rectifying circuit in an extremely wide load range," *IEEE Trans. Microw. Theory Techn.*, vol. 62, no. 4, pp. 986–993, Apr. 2014.

[20] D. Masotti, A. Costanzo, P. Francia, M. Filippi, and A. Romani, "A load-modulated rectifier for RF micropower harvesting with start-up strategies," *IEEE Trans. Microw. Theory Techn.*, vol. 62, no. 4, pp. 994–1004, Apr. 2014.

[21] Y. Huang, N. Shinohara, and T. Mitani, "Impedance matching in wireless power transfer," *IEEE Trans. Microw. Theory Techn.*, vol. 65, no. 2, pp. 582–590, Feb. 2017.

[22] T. Paing, J. Shin, R. Zane, and Z. Popovic, "Resistor emulation approach to low-power RF energy harvesting," *IEEE Trans. Power Electron.*, vol. 23, no. 3, pp. 1494–1501, May 2008.

[23] T. W. Barton, J. M. Gordonson, and D. J. Perreault, "Transmission line resistance compression networks and applications to wireless power transfer," *IEEE Trans. Emerg. Sel. Topics Power Electron.*, vol. 3, no. 1, pp. 252–260, Mar. 2015.

[24] C. Song, Y. Huang, J. Zhou, and P. Carter, "Improved ultrawideband rectennas using hybrid resistance compression technique," *IEEE Trans. Antennas Propag.*, vol. 65, no. 4, pp. 2057–2062, Apr. 2017.

[25] Q. W. Lin and X. Y. Zhang, "Differential rectifier using resistance compression network for improving efficiency over extended input power range," *IEEE Trans. Microw. Theory Techn.*, vol. 64, no. 9, pp. 2943–2954, Sep. 2016.

[26] K. Niotaki, A. Georgiadis, A. Collado, and J. S. Vardakas, "Dual-band resistance compression networks for improved rectifier performance," *IEEE Trans. Microw. Theory Techn.*, vol. 62, no. 12, pp. 3512–3521, Dec. 2014.

[27] C. Song *et al.*, "A novel six-band dual CP rectenna using improved impedance matching technique for ambient RF energy harvesting," *IEEE Trans. Antennas Propag.*, vol. 64, no. 7, pp. 3160–3171, Jul. 2016.

[28] V. Palazzi *et al.*, "A novel ultra-lightweight multiband rectenna on paper for RF energy harvesting in the next generation LTE bands," *IEEE Trans. Microw. Theory Techn.*, vol. 66, no. 1, pp. 366–379, Jan. 2018.

[29] V. Marian, B. Allard, C. Vollaire, and J. Verdier, "Strategy for microwave energy harvesting from ambient field or a feeding source," *IEEE Trans. Power Electron.*, vol. 27, no. 11, pp. 4481–4491, Nov. 2012.

[30] H. Sun, Z. Zhong, and Y.-X. Guo, "An adaptive reconfigurable rectifier for wireless power transmission," *IEEE Microw. Wireless Compon. Lett.*, vol. 23, no. 9, pp. 492–494, Sep. 2013.

[31] J. J. Lu, X.-X. Yang, H. Mei, and C. Tan, "A four-band rectifier with adaptive power for electromagnetic energy harvesting," *IEEE Microw. Wireless Compon. Lett.*, vol. 26, no. 10, pp. 819–821, Oct. 2016.

[32] Z. Liu, Z. Zhong, and Y.-X. Guo, "Enhanced dual-band ambient RF energy harvesting with ultra-wide power range," *IEEE Microw. Wireless Compon. Lett.*, vol. 25, no. 9, pp. 630–632, Sep. 2015.

[33] X. Y. Zhang, Z.-X. Du, and Q. Xue, "High-efficiency broadband rectifier with wide ranges of input power and output load based on branch-line coupler," *IEEE Trans. Circuits Syst. I, Reg. Papers*, vol. 64, no. 3, pp. 731–739, Mar. 2017.

[34] Y.-S. Chen and C.-W. Chiu, "Maximum achievable power conversion efficiency obtained through an optimized rectenna structure for RF energy harvesting," *IEEE Trans. Antennas Propag.*, vol. 65, no. 5, pp. 2305–2317, May 2017.

[35] C. Song *et al.*, "Matching network elimination in broadband rectennas for high-efficiency wireless power transfer and energy harvesting," *IEEE Trans. Ind. Electron.*, vol. 64, no. 5, pp. 3950–3961, May 2017.

[36] A. Collado and A. Georgiadis, "Conformal hybrid solar and electromagnetic (EM) energy harvesting rectenna," *IEEE Trans. Circuits Syst. I, Reg. Papers*, vol. 60, no. 8, pp. 2225–2234, Aug. 2013.

[37] X. Gu *et al.*, "Hybridization of integrated microwave and mechanical power harvester," *IEEE Access*, vol. 6, pp. 13921–13930, 2018.

[38] C. H. P. Lorenz, S. Hemour, W. Liu, A. Badel, F. Formosa, and K. Wu, "Hybrid power harvesting for increased power conversion efficiency," *IEEE Microw. Wireless Compon. Lett.*, vol. 25, no. 10, pp. 687–689, Oct. 2015.

[39] P. Soboll, V. Wienstroer, and R. Kronberger, "Smooth moves in power transition: New Yagi-Uda antenna design for wireless energy," *IEEE Microw. Mag.*, vol. 17, no. 5, pp. 75–80, May 2016.

[40] R. Scheeler, S. Korhummel, and Z. Popovic, "A dual-frequency ultralow-power efficient 0.5-g rectenna," *IEEE Microw. Mag.*, vol. 15, no. 1, pp. 109–114, Jan./Feb. 2014.

[41] A. Mavaddat, S. H. M. Armaki, and A. R. Erfanian, "Millimeter-wave energy harvesting using 4×4 microstrip patch antenna array," *IEEE Antennas Wireless Propag. Lett.*, vol. 14, pp. 515–518, 2015.

[42] Y. Ushijima, T. Sakamoto, E. Nishiyama, M. Aikawa, and I. Toyoda, "5.8-GHz integrated differential rectenna unit using both-sided mic technology with design flexibility," *IEEE Trans. Antennas Propag.*, vol. 61, no. 6, pp. 3357–3360, Jun. 2013.
[43] S. Ladan, A. B. Guntupalli, and K. Wu, "A high-efficiency 24 GHz rectenna development towards millimeter-wave energy harvesting and wireless power transmission," *IEEE Trans. Circuits Syst. I, Reg. Papers*, vol. 61, no. 12, pp. 3358–3366, Dec. 2014.
[44] Y.-J. Ren and K. Chang, "5.8-GHz circularly polarized dual-diode rectenna and rectenna array for microwave power transmission," *IEEE Trans. Microw. Theory Techn.*, vol. 54, no. 4, pp. 1495–1502, Jun. 2006.
[45] H. Sun and W. Geyi, "A new rectenna using beamwidth-enhanced antenna array for RF power harvesting applications," *IEEE Antennas Wireless Propag. Lett.*, vol. 16, pp. 1451–1454, 2017.
[46] H. Sun and W. Geyi, "A new rectenna with all-polarization-receiving capability for wireless power transmission," *IEEE Antennas Wireless Propag. Lett.*, vol. 15, pp. 814–817, 2016.
[47] J.-H. Chou, D.-B. Lin, K.-L. Weng, and H.-J. Li, "All polarization receiving rectenna with harmonic rejection property for wireless power transmission," *IEEE Trans. Antennas Propag.*, vol. 62, no. 10, pp. 5242–5249, Oct. 2014.
[48] J. Kimionis, M. Isakov, B. S. Koh, A. Georgiadis, and M. M. Tentzeris, "3D-printed origami packaging with inkjet-printed antennas for RF harvesting sensors," *IEEE Trans. Microw. Theory Techn.*, vol. 63, no. 12, pp. 4521–4532, Dec. 2015.
[49] E. Vandelle *et al.*, "High gain isotropic rectenna," in *Proc. IEEE Wireless Power Transf. Conf. (WPTC)*, May 2017, pp. 1–4.
[50] D. J. Lee, S.-J. Lee, I.-J. Hwang, W.-S. Lee, and J.-W. Yu, "Hybrid power combining rectenna array for wide incident angle coverage in RF energy transfer," *IEEE Trans. Microw. Theory Techn.*, vol. 65, no. 9, pp. 3409–3418, Sep. 2017.
[51] Y. Y. Hu, H. Xu, H. Sun, and S. Sun, "A high-gain rectenna based on grid-array antenna for RF power harvesting applications," in *Proc. 10th Global Symp. Millim.-Waves*, May 2017, pp. 161–162.
[52] S. Zhang and Y. P. Zhang, "Analysis and synthesis of millimeter-wave microstrip grid-array antennas," *IEEE Antennas Propag. Mag.*, vol. 53, no. 6, pp. 42–55, Dec. 2011.
[53] Z. Chen, Y. P. Zhang, A. Bisognin, D. Titz, F. Ferrero, and C. Luxey, "An LTCC microstrip grid array antenna for 94-GHz applications," *IEEE Antennas Wireless Propag. Lett.*, vol. 14, pp. 1279–1281, 2015.
[54] O. Khan, J. Meyer, K. Baur, and C. Waldschmidt, "Hybrid thin film antenna for automotive radar at 79 GHz," *IEEE Trans. Antennas Propag.*, vol. 65, no. 10, pp. 5076–5085, Oct. 2017.
[55] F. Bauer, X. Wang, W. Menzel, and A. Stelzer, "A 79-GHz radar sensor in LTCC technology using grid array antennas," *IEEE Trans. Microw. Theory Techn.*, vol. 61, no. 6, pp. 2514–2521, Jun. 2013.
[56] M. Nariman, F. Shirinfar, A. P. Toda, S. Pamarti, A. Rofougaran, and F. D. Flaviis, "A compact 60-GHz wireless power transfer system," *IEEE Trans. Microw. Theory Techn.*, vol. 64, no. 8, pp. 2664–2677, Aug. 2016.
[57] J. D. Kraus, "A backward angle-fire array antenna," *IEEE Trans. Antennas Propag.*, vol. AP-12, no. 1, pp. 48–50, Jan. 1964.
[58] J. D. Kraus and R. J. Marhefka, *Antennas for all Applications*, 3rd ed. New York, NY, USA: McGraw-Hill, 2002.
[59] H. Nakano, Y. Iitsuka, and J. Yamauchi, "Rhombic grid array antenna," *IEEE Trans. Antennas Propag.*, vol. 61, no. 5, pp. 2482–2489, May 2013.

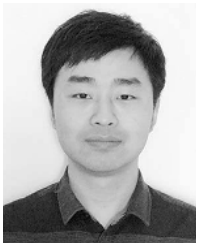

Yi-Yao Hu (S'14) received the B.Eng. degree in electronic engineering from the University of Electronic Science and Technology of China, Chengdu, China, in 2013, where he is currently pursuing the Ph.D. degree.

His current research interests include wireless power transfer and harvesting, rectifying antennas, and power management circuits.

Mr. Hu was a recipient of the Third and Second place awards of the Student Design Competition (Wireless Energy Harvesting) of the IEEE International Microwave Symposium in 2014 and 2015.

Sheng Sun (S'02–M'07–SM'12) received the B.Eng. degree in information engineering from Xi'an Jiaotong University, Xi'an, China, in 2001, and the Ph.D. degree in electrical and electronic engineering from Nanyang Technological University (NTU), Singapore, in 2006.

From 2005 to 2006, he was with the Institute of Microelectronics, Singapore. From 2006 to 2008, he was a Post-Doctoral Research Fellow with NTU. From 2008 to 2010, he was a Humboldt Research Fellow with the Institute of Microwave Techniques, University of Ulm, Ulm, Germany. From 2010 to 2015, he was a Research Assistant Professor with The University of Hong Kong, Hong Kong. Since 2015, he has been a Full Professor with the University of Electronic Science and Technology of China, Chengdu, China. He has authored or co-authored 1 book and 2 book chapters, and over 140 journal and conference publications. His current research interests include electromagnetic theory, computational mathematics, multiphysics, numerical modeling of planar circuits and antennas, microwave passive and active devices, and the microwave- and millimeter-wave communication systems.

Dr. Sun is currently a member of the Editor Board of the *International Journal of RF and Microwave Computer Aided Engineering* and the *Journal of Communications and Information Networks*. He was a recipient of the ISAP Young Scientist Travel Grant, Japan, in 2004, the Hildegard Maier Research Fellowship of the Alexander Von Humboldt Foundation, Germany, in 2008, the Outstanding Reviewer Award of the IEEE MICROWAVE AND WIRELESS COMPONENTS LETTERS in 2010, and the General Assembly Young Scientists Award from the International Union of Radio Science in 2014. He was a co-recipient of the several Best Paper Awards of international conferences. He was an Associate Editor of the *IEICE Transactions on Electronics* from 2010 to 2014 and a Guest Associate Editor of the *Applied Computational Electromagnetics Society Journal* in 2017. He serves as an Associate Editor for IEEE MICROWAVE AND WIRELESS COMPONENTS LETTERS.

Hao Xu was born in Shenyang, China. He received the B.S. degree in electromagnetic field and radio technology from the University of Electronic Science and Technology of China, Chengdu, China, in 2015, where he is currently pursuing the M.E. degree in electronics and communication engineering.

His current research interests include differentially fed antennas and rectennas.

Hucheng Sun (M'14) received the B.Eng. degree in electronic engineering and information science from the University of Science and Technology of China, Hefei, China, in 2009, and the Ph.D. degree in electromagnetic field and microwave engineering from the National University of Singapore, Singapore, in 2014.

In 2014, he was a Research Assistant with The University of Hong Kong (HKU), Hong Kong, China, where he was a Post-Doctoral Fellow in 2015. Since 2014, he has been a Lecturer with the Nanjing University of Information Science and Technology, Nanjing, China. His current research interests include antennas and wave propagation, microwave circuit, and wireless power.

Dr. Sun was a recipient of the 2015 Jiangsu Innovative and Entrepreneurial Doctor, the Best Student Paper Award of the 2013 IEEE International Workshop on Electromagnetics, Hong Kong, China. He serves as a Reviewer for several IEEE journals and other international journals.